Dye-Sensitized Solar Cells

DOI: 10.1002/anie.201400388

Podlike N-Doped Carbon Nanotubes Encapsulating FeNi Alloy Nanoparticles: High-Performance Counter Electrode Materials for Dye-Sensitized Solar Cells**

Xiaojia Zheng, Jiao Deng, Nan Wang, Dehui Deng, Wen-Hua Zhang,* Xinhe Bao, and Can Li*

Dedicated to Professor Dongsheng Yan on the occasion of his 96th birthday

Abstract: *Podlike nitrogen-doped carbon nanotubes encapsulating FeNi alloy nanoparticles (Pod(N)-FeNi) were prepared by the direct pyrolysis of organometallic precursors. Cyclic voltammetry (CV), electrochemical impedance spectroscopy (EIS), and Tafel polarization measurements revealed their excellent electrocatalytic activities in the I^-/I_3^- redox reaction of dye-sensitized solar cells (DSSCs). This is suggested to arise from the modification of the surface electronic properties of the carbon by the encapsulated metal alloy nanoparticles (NPs). Sequential scanning with EIS and CV further showed the high electrochemical stability of the Pod(N)-FeNi composite. DSSCs with Pod(N)-FeNi as the counter electrode (CE) presented a power conversion efficiency of 8.82 %, which is superior to that of the control device with sputtered Pt as the CE. The Pod(N)-FeNi composite thus shows promise as an environmentally friendly, low-cost, and highly efficient CE material for DSSCs.*

Dye-sensitized solar cells (DSSCs) offer one of the possibilities to address the ever-increasing challenge for clean energy due to their high efficiency and low-cost fabrication.[1] Studies on DSSCs have progressed to such a level that industrial application of DSSCs is currently in its initial stage.[2] In a DSSC, a counter electrode (CE) with both high electrical conductivity and excellent electrocatalytic activity is indispensable for obtaining excellent performance and high efficiency.[1b] In this regard, Pt is the most useful CE material with the above-mentioned characteristics, and contributes to the excellent efficiency of the DSSCs. However, as a noble metal, Pt is very expensive, which hinders seriously its use in the large-scale fabrication of DSSCs. Therefore, alternatives are necessary for the fabrication of low-cost and high-performance CEs of DSSCs. So far, several kinds of new materials have been proposed, such as conductive organic polymers,[3] inorganic oxides,[4] sulfides,[5] selenides,[6] nitrides,[4b] carbides,[4b,7] and carbon materials. Among them, carbon materials are of particular interest due to the very abundant source, environmentally benign nature, low-cost fabrication, and good electrochemical catalytic activity. Carbon black,[8] carbon nanotubes (CNTs),[8b,9] and graphene[9d,10] have been successfully applied as CEs of DSSCs in a number of studies. Nevertheless, up to now the performance of the DSSCs with carbon CEs has not been satisfactory and is usually inferior to that of DSSCS with Pt as the CE.[8,9,10c] Hence, it remains a challenge to seek for a carbon-based CE material with excellent performance for the further development of DSSCs.

Recently, we have reported a novel strategy for the in situ encapsulation of Fe nanoparticles (NPs) within podlike carbon nanotubes (designated as Pod-Fe) by a direct chemical synthesis method.[11] The materials obtained displayed excellent catalytic activity for the oxygen reduction reaction (ORR) and good durability in polymer electrolyte membrane fuel cells (PEMFCs). Inspired by this, we report herein on the preparation of podlike N-doped CNTs with encapsulated FeNi alloy NPs (Pod(N)-FeNi) by the direct pyrolysis of organometallic precursors and on their application as CEs in DSSCs. Experimental results demonstrated that the Pod(N)-FeNi composite showed better catalytic activity towards reducing I_3^- than the sputtered Pt, and the DSSC device made from the Pod(N)-FeNi CE displayed a power conversion efficiency (PCE) of 8.82 %, outperforming the control device containing the sputtered Pt CE (8.01 % PCE).

Pod(N)-FeNi was prepared using $[Ni_2Fe(CN)_6]$ as the precursor by calcinating at 600 °C in an Ar atmosphere. The sample obtained was treated with 1.0 M H_2SO_4 aqueous solution to remove the metal residue on the external surface of the carbon material, resulting in the Pod(N)-FeNi composite. Scanning electron microscopy (SEM) images reveals the tubular structures of the Pod(N)-FeNi and the presence of metal NPs at the ends of nanotubes (Figure 1 a). X-ray diffraction (XRD) patterns of the materials show diffraction peaks located at $2\theta = 26.4$, 43.7, 51.0, and 74.7°, attributable to the (002) lattice planes of graphite (JCPDS 41-1487), and

[*] X. J. Zheng,[+] J. Deng,[+] N. Wang, Prof. D. H. Deng, Prof. W.-H. Zhang, Prof. X. H. Bao, Prof. C. Li
State Key Laboratory of Catalysis
Dalian Institute of Chemical Physics
Chinese Academy of Sciences
Dalian National Laboratory for Clean Energy, Dalian 116023 (China)
E-mail: dhdeng@dicp.ac.cn
whzhang@dicp.ac.cn

[+] These authors contributed equally to this work.

[**] We thank Prof. T. L. Ma at Dalian University of Technology for fruitful discussions on counter electrodes in DSSCs and gratefully acknowledge financial support from the "Hundred Talents Program" of the Chinese Academy of Sciences, the National Science Foundation of China (nos. 20873141 and 21303191), and the Strategic Priority Research Program of the Chinese Academy of Sciences (no. XDA09030100).

Supporting information for this article is available on the WWW under http://dx.doi.org/10.1002/anie.201400388.

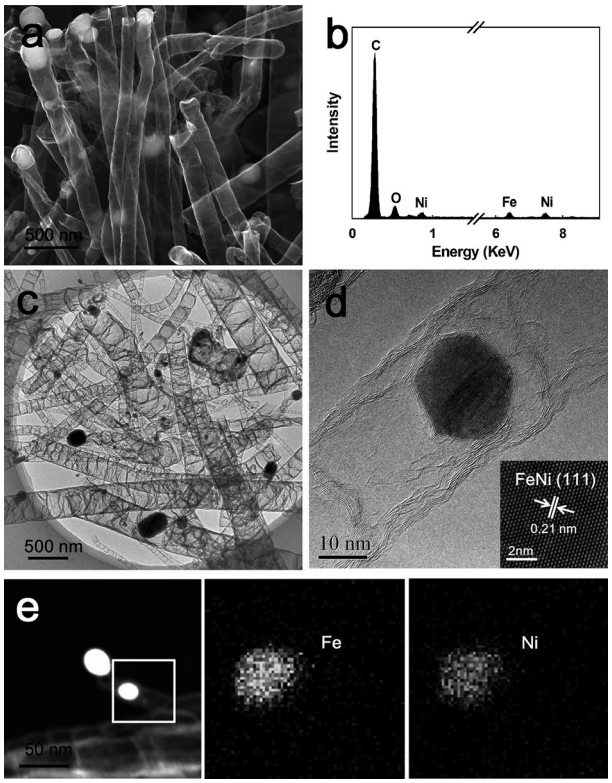

Figure 1. a) SEM images, b) EDS analysis, c) TEM image, d) HRTEM image of the Pod (N)-FeNi (inset: HRTEM image of the FeNi alloy nanoparticle), and e) elemental mapping of the materials (the area in the box) reveal the homogeneous distribution of Ni and Fe elements in the metal NPs.

to the (111), (200), and (220) planes of the FeNi alloy (JCPDS 03-1209) (Figure S1), respectively. X-ray photoelectron spectroscopy (XPS) disclosed the presence of nitrogen in the sample and the metallic nature of the FeNi alloy of the encapsulated NPs (Figure S2). The presence of Ni and Fe was further confirmed by energy-dispersive X-ray spectroscopy (EDS) analysis (Figure 1b). Transmission electron microscopy (TEM) of the Pod(N)-FeNi showed a well-defined podlike structure with large metal NPs located at the ends of the nanotubes (Figure 1c, Figure S3). High-resolution TEM (HRTEM) images of the large metal NP presented 0.21 nm lattice fringes, which can be attributed to the (111) lattice plane of the FeNi alloy (inset of Figure 1d), in line with the above XRD results. Elemental mapping of one metal nanoparticle showed a homogeneous distribution of both Fe and Ni around the nanoparticle (Figure 1e), further confirming the alloy nature of the FeNi NPs in the sample obtained. Besides the large FeNi NPs, many smaller metal NPs were also observed in the compartments of the Pod(N)-FeNi by HRTEM and high-angle annular dark-field (HAADF) spectroscopy (Figures S4 and S5). These results demonstrate that podlike graphitic nitrogen-doped carbon nanotubes encapsulating FeNi alloy NPs were successfully prepared. The obtained Pod(N)-FeNi was then ultrasonically dispersed in isopropanol for 30 min resulting in a Pod(N)-FeNi slurry, which was subsequently sprayed onto fluorine-doped tin oxide (FTO) glass to form the Pod(N)-FeNi counter electrode of DSSCs for further study.

To examine the catalytic activities of the Pod(N)-FeNi and Pt CEs toward the reduction of I_3^- in the I^-/I_3^- redox shuttle of the DSSCs, cyclic voltammetry (CV) was performed in an acetonitrile solution containing 10 mM LiI, 1 mM I_2, and 0.1M $LiClO_4$ at a scanning rate of 50 mV s^{-1}. Identical conditions were used for measurements with the Pt CE for comparison purposes (Figure 2a). Both electrodes exhibit two typical pairs of oxidation/reduction peaks (Ox-A/Red-A, Ox-B/Red-B). The Ox-A/Red-A pair in the CV plots is assigned to the oxidation and reduction of I^-/I_3^-, whereas the Ox-B/Red-B pair to the oxidation and reduction of I_3^-/I_2. The peak current and peak separation between the anodic and cathodic peaks (Epp) are very useful parameters for assessing the catalytic activity of a CE,[6b] whilst Epp is negatively correlated with the standard electrochemical rate constant of a redox reaction. The Epp of the Pod(N)-FeNi CE (ca. 60 mV) is significantly smaller than that of the Pt electrode (140 mV) and is directly responsible for the fact that the overpotential loss of the Pod(N)-FeNi CE is lower than that of the Pt CE in DSSCs. Higher peak current densities and lower Epp values (Figure 2a) suggest that the Pod(N)-FeNi electrode presents high catalytic activity in the reduction of I_3^-, which is a paramount prerequisite for an excellent CE in DSSCs.

We have further compared the cyclic voltammograms recorded at different scanning rates for the Pod(N)-FeNi and Pt electrodes (shown in Figures S6 and S7) to extract the relationship between the scanning rates and the peak current densities of Ox-A/Red-A (Figure 2b). The peak current densities increased with increasing scanning rates, and a linear relationship was found between the peak current densities and the square root of the scanning rates. Such a linear relationship indicates that the cathodic and anodic reactions are diffusion limited for the transportation of iodide species toward the counter electrode in the cells. This is

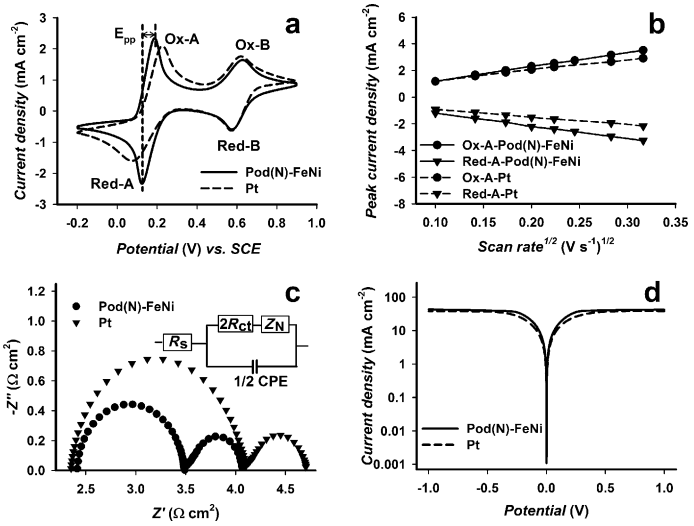

Figure 2. a) Cyclic voltammograms, b) relationship between the peak current density for the I^-/I_3^- redox reaction and the square root of scanning rate of the Pod(N)-FeNi and the sputtered Pt CEs. c) Electrochemical impedance spectra and d) Tafel polarization curves of symmetrical cells.

because of the fact that, as the scanning rate increases, the diffusion layer becomes thinner and the electrochemical polarization becomes larger, thus leading to a high overpotential and poor reversibility.[12]

Electrochemical impedance spectroscopy (EIS) represents the intrinsic interfacial charge transfer and charge transport kinetics at the electrode/electrolyte interface. We performed EIS using symmetrical cells consisting of two identical CEs and investigated the charge transfer process at the electrode/electrolyte interface. The obtained Nyquist plots of the two electrodes are presented in Figure 2c. The high-frequency intercept on the real axis corresponds to series resistance (R_S) of the cell, while the charge transfer resistance (R_{ct}) at the electrode/electrolyte interface for the I_3^- reduction and the corresponding constant phase angle element (CPE) can be revealed by the left semicircle in the high-frequency range. Additionally, the right semicircle in the low-frequency range reflects the Nernst diffusion impedance (Z_N) of the redox couple transport in the electrolyte. The Nyquist plots for the two CEs were fitted by the Z-view software with an equivalent circuit diagram (inset of Figure 2c), producing the EIS parameters shown in Table S1. The two electrodes yielded very similar R_S values, hence posing a similar influence on the photovoltaic performance of the respective devices using the Pod(N)-FeNi and the Pt CEs. The R_{ct} value of the Pod(N)-FeNi is 0.54 $\Omega\,cm^2$, smaller than the value of 0.88 $\Omega\,cm^2$ for the Pt CE (Table S1). This indicates that the Pod(N)-FeNi electrode has higher catalytic activity than the sputtered Pt electrode in the reduction of I_3^- in DSSCs. Effective reduction of I_3^- to I^- could promote the dye regeneration at the photoanode, resulting in an improvement of photocurrent density (J_{sc}). Meanwhile, a lower R_{ct} would lead to lower series resistance, which would improve the fill factor of solar cells.[10e,13]

Tafel polarization was employed to further elucidate the catalytic activity of CEs for DSSCs. Figure 2d shows Tafel curves of symmetrical cells based on the Pod(N)-FeNi and Pt CEs, respectively. Both the anodic and cathodic branches showed larger slopes for the Pod(N)-FeNi electrode than for the Pt electrode, suggesting higher exchange current density (J_0) generated from the Pod(N)-FeNi electrode. This is in line with the EIS values in terms of Equation (1), where R is the gas constant, T is the

$$J_0 = \frac{RT}{nFR_{ct}} \quad (1)$$

temperature, F is the Faraday constant, n is the number of electrons involved in the reduction, and R_{ct} is the charge transfer resistance.

Figure 2d further shows very similar limiting diffusion current density (J_{lim}) values for the Pod(N)-FeNi and Pt electrodes, indicative of very similar diffusion coefficients in the symmetrical cells according to Equation (2), where D is the diffusion

$$D = \frac{l}{2nFC}J_{lim} \quad (2)$$

coefficient, l is the distance between electrodes in a dummy cell, n is the number of electrons involved in the reduction of triiodide at the electrode, F is the Faraday constant, and C is the I_3^- concentration.

Taking the above results into consideration, including EIS, CV, and Tafel polarization, the Pod(N)-FeNi catalyst displayed high catalytic activity towards the reducing of I_3^-, which is even better than that of the sputtered Pt electrode, which is currently the most frequently used high-performance CE material in DSSCs.

The electrochemical stability of a CE is an important parameter affecting the potential application of DSSCs. To assess the electrochemical stability of the Pod(N)-FeNi as a CE of DSSCs, two symmetrical cells containing the Pod(N)-FeNi and sputtered Pt electrodes, respectively, were subjected to sequential scanning of CV and EIS for 10 cycles. Changes in R_{ct} were negligible for both CEs after 10 cycles of scanning, showing the superior electrochemical stability of both electrodes (Figure 3a,c). Moreover, there were almost no changes in R_s and Z_N for the two cells subjected to repeated scanning cycles, implying that the potential cycling exerts trivial influence on the series resistance and the mass transport in the redox electrolyte solution. We also measured sequential CV for 150 cycles for both of the CEs. The current densities and the Epp had nearly no change for the Pod(N)-FeNi electrode (Figure 3b), while for the Pt electrode subjected to the same scanning, the reduction peak current density decreased and the Epp increased noticeably (Figure 3d). These results demonstrated the excellent stability of the Pod(N)-FeNi CE, which can be attributed to the fact that the NiFe alloy NPs were encapsulated within the tubes of the

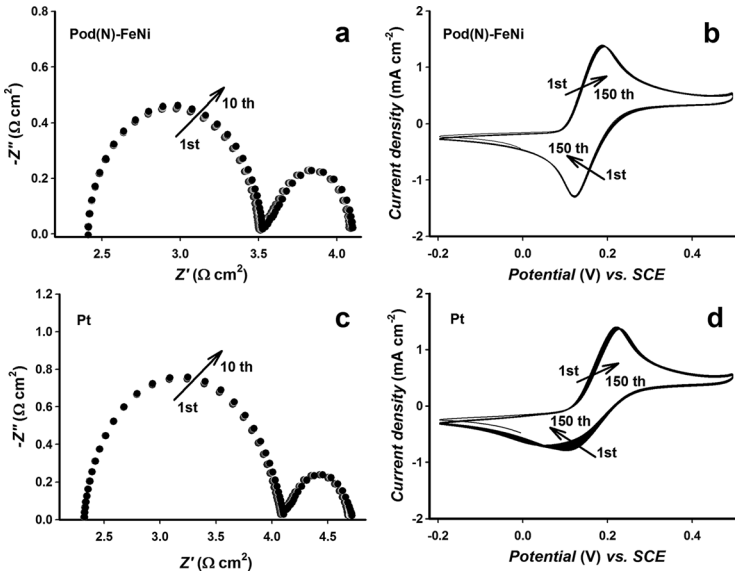

Figure 3. a,c) Nyquist plots of EIS data for the symmetrical cells with Pod(N)-FeNi (a) and sputtered Pt electrodes (c). b,d) Sequential cyclic voltammograms for Pod(N)-FeNi and d sputtered Pt CEs. The cells were first subjected to CV scanning (from 0 V→1 V→−1 V→0 V at a scanning rate of 100 $mV\,s^{-1}$), followed by 60 s relaxation at 0 V, and then EIS measurement was performed at 0 V from 0.01 Hz to 400 kHz. This sequential electrochemical test was repeated 10 times. A total of 150 consecutive cyclic voltammograms were recorded for the I^-/I_3^- system at a scanning rate of 20 $mV\,s^{-1}$ for Pod(N)-FeNi (b) and sputtered Pt (d) CEs.

CNT hosts and thus protected from leaching and corrosion caused by the electrolyte.

The excellent catalytic activity in the I^-/I_3^- redox reaction and the high electrochemical stability of the Pod(N)-FeNi composite make it potentially very suitable to use as a CE for DSSCs. To directly assess this, DSSC devices were fabricated using Pod(N)-FeNi and sputtered Pt as CEs (see the Supporting Information). Figure 4 shows the comparison of

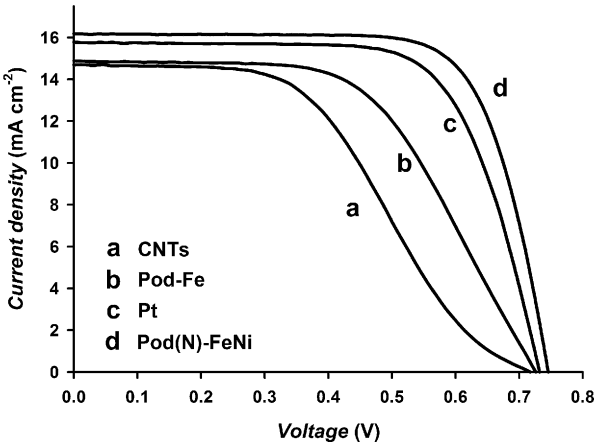

Figure 4. Photocurrent density versus voltage (*J*–*V*) curves of the DSSCs using CNTs (a), Pod-Fe (b), Pt (c), and Pod(N)-FeNi (d) as CEs.

the photocurrent density–voltage (*J*–*V*) characteristics of the two devices, and the corresponding photovoltaic parameters are summarized in Table 1. The Pod(N)-FeNi-based device displayed higher open circuit voltage ($V_{oc} = 745$ mV), larger short-circuit current ($J_{sc} = 16.2$ mA cm^{-2}) and better fill factor

Table 1: Photovoltaic performance of the DSSCs.

CE	V_{oc} [mV]	J_{sc} [mA cm^{-2}]	FF [%]	PCE [%]
CNTs	715	14.69	46.36	4.87
Pod-Fe	725	14.88	56.73	6.12
Pod(N)-FeNi	745	16.16	73.21	8.82
Pt	730	15.76	69.55	8.01

(73.2 %) than the Pt device ($V_{oc} = 730$ mV, $J_{sc} = 15.8$ mA cm^{-2}, fill factor of 69.6 %). Thus a PCE of 8.82 % was achieved for the Pod(N)-FeNi device, which is superior to the 8.01 % PCE for the Pt-based device. Therefore, all the main photovoltaic parameters (V_{oc}, J_{sc}, fill factor) were responsible for the excellent performance of the Pod(N)-FeNi cell, which apparently arises from the good conductivity of the graphitic carbon and the excellent catalytic activity of the Pod(N)-FeNi in the I^-/I_3^- redox reaction.

Moreover, we have also evaluated the catalytic performance of pristine CNTs and podlike CNTs encapsulating iron (Pod-Fe) as CEs of DSSCs (Figures S8–10). It can be found that the performance of the devices using CNTs or Pod-Fe as CEs is significantly inferior to that of the Pod(N)-FeNi-based cell (Figure 4). Pristine carbon materials usually exhibit a good electrical conductivity but offer limited catalytic active sites due to their chemical inertness.[10f] In contrast to pristine CNTs, the existence of metal nanoparticles within the CNTs can promote the electron transfer from the metal to the carbon walls, which can change the electronic structure and reduce the surface work function of the carbon walls, consequently enhancing the catalytic activity of the carbon walls.[11,14] Furthermore, it has been demonstrated that nitrogen doping into the carbon network can further promote the charge transfer and reduce the local work function of the CNTs,[11,14a] and can also introduce more electrocatalytic active cites and enhance hydrophilicity to strengthen electrolyte–electrode interaction.[10c,15] Therefore, both the encapsulated FeNi NPs and the doped N atoms in the CNTs exert a synergistically favorable influence on the CE performance of the Pod(N)-FeNi in this study. The pristine CNTs show the lowest performance, while the Pod(N)-FeNi presents the highest performance of the CEs studied herein.

In summary, podlike N-doped carbon nanotubes encapsulating FeNi alloy NPs were prepared by the direct pyrolysis of $[Ni_2Fe(CN)_6]$ in an inert atmosphere and exhibited excellent electrocatalytic performance in the I^-/I_3^- redox reaction in DSSCs. The Pod(N)-FeNi catalyst displayed significantly lower peak separation between the anodic and cathodic peaks (Epp), lower charge transfer resistance (R_{ct}) at the interface of the CE/electrolyte, higher exchange current density, and better electrochemical stability under prolonged cycling than the sputtered Pt counterpart. Notably, the DSSC devices consisting of the Pod(N)-FeNi CE displayed a power conversion efficiency (PCE) of 8.82 %, superior to that of the control device using sputtered Pt as the CE (PCE = 8.01 %). These results may pave the way for the further study of environmentally friendly, stable, economical, and highly efficient counter electrodes for DSSCs.

Received: January 14, 2014
Published online: May 5, 2014

Keywords: carbon nanotubes · electrocatalysis · FeNi alloys · non-precious metals · solar cells

[1] a) B. O'Regan, M. Grätzel, *Nature* **1991**, *353*, 737; b) A. Hagfeldt, G. Boschloo, L. Sun, L. Kloo, H. Pettersson, *Chem. Rev.* **2010**, *110*, 6595.
[2] M. Grätzel, *Acc. Chem. Res.* **2009**, *42*, 1788.
[3] a) H. Tian, Z. Yu, A. Hagfeldt, L. Kloo, L. Sun, *J. Am. Chem. Soc.* **2011**, *133*, 9413; b) K.-M. Lee, W.-H. Chiu, H.-Y. Wei, C.-W. Hu, V. Suryanarayanan, W.-F. Hsieh, K.-C. Ho, *Thin Solid Films* **2010**, *518*, 1716; c) H. N. Tsao, J. Burschka, C. Yi, F. Kessler, M. K. Nazeeruddin, M. Gratzel, *Energy Environ. Sci.* **2011**, *4*, 4921.
[4] a) Y. Hou, D. Wang, X. H. Yang, W. Q. Fang, B. Zhang, H. F. Wang, G. Z. Lu, P. Hu, H. J. Zhao, H. G. Yang, *Nat. Commun.* **2013**, *4*, 1583; b) M. Wu, X. Lin, Y. Wang, L. Wang, W. Guo, D. Qi, X. Peng, A. Hagfeldt, M. Grätzel, T. Ma, *J. Am. Chem. Soc.* **2012**, *134*, 3419.
[5] a) X. Xin, M. He, W. Han, J. Jung, Z. Lin, *Angew. Chem.* **2011**, *123*, 11943; *Angew. Chem. Int. Ed.* **2011**, *50*, 11739; b) X. Zheng, J. Guo, Y. Shi, F. Xiong, W.-H. Zhang, T. Ma, C. Li, *Chem. Commun.* **2013**, *49*, 9645; c) L. Yi, Y. Liu, N. Yang, Z. Tang, H.

Zhao, G. Ma, Z. Su, D. Wang, *Energy Environ. Sci.* **2013**, *6*, 835; d) Y.-C. Wang, D.-Y. Wang, Y.-T. Jiang, H.-A. Chen, C.-C. Chen, K.-C. Ho, H.-L. Chou, C.-W. Chen, *Angew. Chem.* **2013**, *125*, 6826; *Angew. Chem. Int. Ed.* **2013**, *52*, 6694.

[6] a) F. Gong, X. Xu, Z. Li, G. Zhou, Z.-S. Wang, *Chem. Commun.* **2013**, *49*, 1437; b) F. Gong, H. Wang, X. Xu, G. Zhou, Z.-S. Wang, *J. Am. Chem. Soc.* **2012**, *134*, 10953.

[7] M. Wu, X. Lin, A. Hagfeldt, T. Ma, *Angew. Chem.* **2011**, *123*, 3582; *Angew. Chem. Int. Ed.* **2011**, *50*, 3520.

[8] a) T. N. Murakami, S. Ito, Q. Wang, M. K. Nazeeruddin, T. Bessho, I. Cesar, P. Liska, R. Humphry-Baker, P. Comte, P. Pechy, M. Grätzel, *J. Electrochem. Soc.* **2006**, *153*, A2255; b) M. Wu, X. Lin, T. Wang, J. Qiu, T. Ma, *Energy Environ. Sci.* **2011**, *4*, 2308.

[9] a) Z. Yang, T. Chen, R. He, G. Guan, H. Li, L. Qiu, H. Peng, *Adv. Mater.* **2011**, *23*, 5436; b) J. Han, H. Kim, D. Y. Kim, S. M. Jo, S.-Y. Jang, *Acs Nano* **2010**, *4*, 3503; c) F. Malara, M. Manca, M. Lanza, C. Huebner, E. Piperopoulos, G. Gigli, *Energy Environ. Sci.* **2012**, *5*, 8377; d) Z. Yang, M. Liu, C. Zhang, W. W. Tjiu, T. Liu, H. Peng, *Angew. Chem.* **2013**, *125*, 4088; *Angew. Chem. Int. Ed.* **2013**, *52*, 3996.

[10] a) M. J. Ju, J. C. Kim, H.-J. Choi, I. T. Choi, S. G. Kim, K. Lim, J. Ko, J.-J. Lee, I.-Y. Jeon, J.-B. Baek, H. K. Kim, *ACS Nano* **2013**, *7*, 5243; b) L. Kavan, J.-H. Yum, M. K. Nazeeruddin, M. Grätzel, *Acs Nano* **2011**, *5*, 9171; c) Y. Xue, J. Liu, H. Chen, R. Wang, D. Li, J. Qu, L. Dai, *Angew. Chem.* **2012**, *124*, 12290; *Angew. Chem. Int. Ed.* **2012**, *51*, 12124; d) F. Gong, H. Wang, Z.-S. Wang, *Phys. Chem. Chem. Phys.* **2011**, *13*, 17676; e) S. Hou, X. Cai, H. Wu, X. Yu, M. Peng, K. Yan, D. Zou, *Energy Environ. Sci.* **2013**, *6*, 3356; f) J. D. Roy-Mayhew, D. J. Bozym, C. Punckt, I. A. Aksay, *Acs Nano* **2010**, *4*, 6203.

[11] D. Deng, L. Yu, X. Chen, G. Wang, L. Jin, X. Pan, J. Deng, G. Sun, X. Bao, *Angew. Chem.* **2013**, *125*, 389; *Angew. Chem. Int. Ed.* **2013**, *52*, 371.

[12] M. Wu, Y. Wang, X. Lin, N. Yu, L. Wang, L. Wang, A. Hagfeldt, T. Ma, *Phys. Chem. Chem. Phys.* **2011**, *13*, 19298.

[13] S. Das, P. Sudhagar, V. Verma, D. Song, E. Ito, S. Y. Lee, Y. S. Kang, W. Choi, *Adv. Funct. Mater.* **2011**, *21*, 3729.

[14] a) J. Deng, L. Yu, D. Deng, X. Chen, F. Yang, X. Bao, *J. Mater. Chem. A* **2013**, *1*, 14868; b) Y. Hu, J. O. Jensen, W. Zhang, L. N. Cleemann, W. Xing, N. J. Bjerrum, Q. Li, *Angew. Chem.* **2014**, DOI: 10.1002/ange.201400358; *Angew. Chem. Int. Ed.* **2014**, DOI: 10.1002/anie.201400358.

[15] a) S. Yang, X. Feng, X. Wang, K. Müllen, *Angew. Chem.* **2011**, *123*, 5451; *Angew. Chem. Int. Ed.* **2011**, *50*, 5339; b) D. Yu, E. Nagelli, F. Du, L. Dai, *J. Phys. Chem. Lett.* **2010**, *1*, 2165; c) D. S. Su, J. Zhang, B. Frank, A. Thomas, X. Wang, J. Paraknowitsch, R. Schlögl, *ChemSusChem* **2010**, *3*, 169.

